Evidence for possible flexoelectricity in tobacco mosaic viruses used as nanotemplates

Sergei V. Kalinin[a] and Stephen Jesse
Condensed Matter Sciences Division, Oak Ridge National Laboratory, Oak Ridge, Tennessee 37831

Weili Liu and Alexander A. Balandin[b]
Nano-Device Laboratory, Department of Electrical Engineering, University of California-Riverside, Riverside, California 92521

(Received 19 October 2005; accepted 1 March 2006; published online 11 April 2006)

Electromechanical coupling in individual tobacco mosaic viruses has been studied using piezoresponse force microscopy. Possible origins of the observed high resolution contrast, including the topographic crosstalk, difference in the elastic properties, and the intrinsic electromechanical coupling due to the piezoelectric and flexoelectric effects are discussed. Using simple estimates, we argue that, due in part to the small size and high symmetry of this particular material system, flexoelectric coupling can dominate the observed electromechanical behavior. The electrical manipulation of the virus particles, essential for nanoelectronic applications for which they are proposed, has also been demonstrated. © *2006 American Institute of Physics*.
[DOI: 10.1063/1.2194008]

Electromechanical coupling is a nearly universal feature of most biopolymers since it is strongly correlated with the presence of optical activity and polar bonds.[1] Recently, local electromechanical coupling has been observed in a variety of biosystems and imaged with sub–10 nm resolution, providing unprecedented insight into the nanostructure of these materials.[2,3] Traditionally, electromechanical coupling is due to the piezoelectric effect, i.e. the linear coupling between electric field and strain. However, in nanoscale systems, the flexoelectric effect, in which electric field and the *gradient of the strain* are linearly coupled, can play a substantial role.[4] This behavior is nearly universal in objects such as cellular membranes, in which regions with smaller radius of curvature have higher dipole moment and hence stronger electromechnical response.[5] While in bulk materials piezoelectric coupling is relatively weak, the presence of large strain gradients on the nanoscale can make flexoelectric contribution comparable to or, for centrosymmetric systems, dominant in the overall electromechanical response.

In this letter, we report on the application of piezoresponse force microscopy (PFM) to study tobacco mosaic plant viruses (TMVs), which have recently been proposed as nanotemplates for the chemical assembly of nanoelectronic circuit elements.[6–8] TMV is a robust rod-shaped virus with dimensions suitable for nanofabrication: it is 300 nm long, 18 nm in diameter, and has a 4 nm axial channel. This virus can form end-to-end assemblies, required for nanowire interconnect fabrication, and can be coated with metals and semiconductor materials. TMVs used in this study were grown on Nicotiana tabacum "Xanthi" plants. After extraction and required processing, the TMV solution was deposited on freshly cleaved mica disks, wicked, and air dried. Details of the TMV preparation are reported elsewhere.[8]

In PFM, a conductive tip is brought into contact with the surface, and the piezoelectric response is detected as the first harmonic component, $A_{1\omega}$, of the tip deflection, $A=A_0+A_{1\omega}\cos(\omega t+\varphi)$, induced by the application of the periodic bias, $V_{\mathrm{tip}}=V_{\mathrm{dc}}+V_{ac}\cos(\omega t)$, to the tip. The principles and image formation mechanisms of PFM are described in detail elsewhere.[9–11] PFM is implemented on a commercial scanning probe microscopy system (Veeco MultiMode NS-IIIA) equipped with additional function generators and lock-in amplifiers (DS 345 and SRS 830, Stanford Research Instruments, and Model 7280, Signal Recovery). A custom-built sample holder was used to allow direct tip biasing and to avoid crosstalk with the microscope electronics. In order to enable imaging of the relatively fragile surface and minimize virus motion during scanning in contact mode, measurements were performed using soft cantilevers (Pt and Au coated tips, NCSC-12 C, Micromasch, $l\approx 130$ μm, spring constant $k\sim 0.16$ N/m). Typically, imaging was performed in the vicinity of high-order cantilever resonances ($\sim$650 kHz) to increase the signal-to-noise ratio.

The surface topography illustrating a continuous network of the viral particles is shown in Figs. 1(a), 1(c), and 1(e). Note that despite the fact that imaging is performed in the contact mode the surface damage is minimal and reproducible images from the same region can be obtained. The radius of the virus as extracted from atomic force microscopy (AFM) data is $a=9$ nm. The agreement between the measured and the expected radius, as well as reproducibility of the images after repetitive scans, indicates that the tip damage to TMVs is minimal, even in contact mode. The apparent half-width at half maximum, $H=52$ nm, is significantly larger than the virus radius due to tip-surface convolution. Using the geometric identity $H=2\sqrt{Ra}$, the tip radius of curvature is estimated to be $R=80$ nm. For comparison, Figs. 1(b), 1(d), and 1(f) show the corresponding PFM images. On a large scan [Fig. 1(b)], PFM contrast is clearly visible—effectively distinguishing the viral network from the substrate. In high resolution images, the PFM maps contain multiple features invisible in the topographic scans, thus

[a]Author to whom correspondence should be addressed; electronic mail: sergei2@ornl.gov
[b]On leave from: Department of Engineering, University of Cambridge, Cambridge CB2 1PZ, United Kingdom.

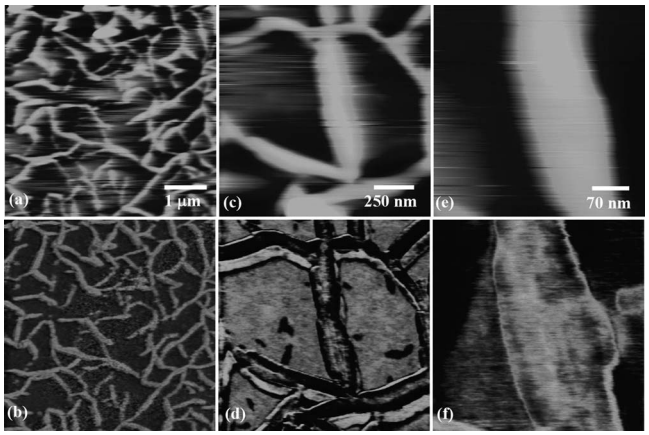

FIG. 1. Surface topography [(a), (c), and (e)] and piezoresponse images [(b), (d), and (f)] of tobacco mosaic virus at different resolutions.

demonstrating the potential of PFM for high resolution studies of such biosystems.

The resolution observed in the PFM is below that achievable in intermittent- and noncontact AFMs, when individual protein molecules can be resolved.[12,13] However, in these techniques, the electrostatic interactions will dominate the signal. Hence, electromechanical imaging necessitates contact mode operation.

A plot of the measured linear dependence of PFM contrast on driving voltage is shown in Fig. 2. This linear behavior is consistent with either the piezo- or flexoelectric effect. Note that with the available information, unambiguous interpretation of the observed PFM contrast in terms of intrinsic electromechanical response of the material is not possible. The use of relatively soft cantilevers and high PFM driving frequencies (above the cantilever resonance) can give rise to (a) crosstalk between topography and the PFM signal and (b) contrast due to variations in elastic properties between the virus and substrate and hence variations in the magnitude of electrostatically driven tip oscillations. And, while these considerations can not be ruled out from the scanning probe microscopy (SPM) data, here we analyze the possible sources of electromechanical contrast in virus particles and demonstrate that their measurable effects are well within the detection limits of PFM.

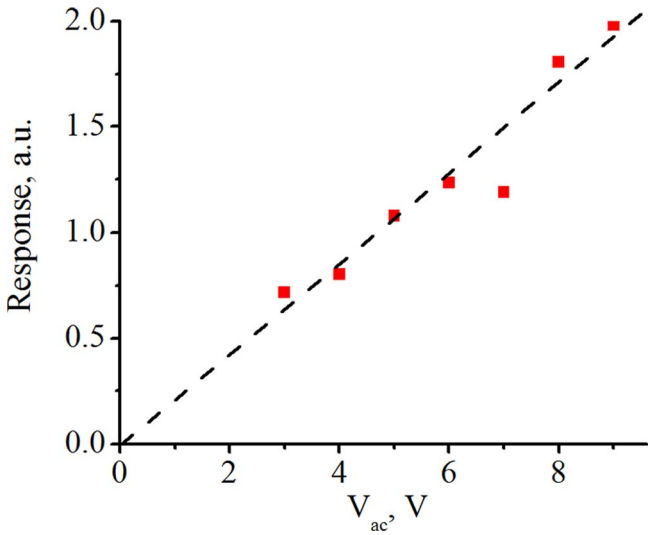

FIG. 2. Driving bias dependence of PFM. contrast.

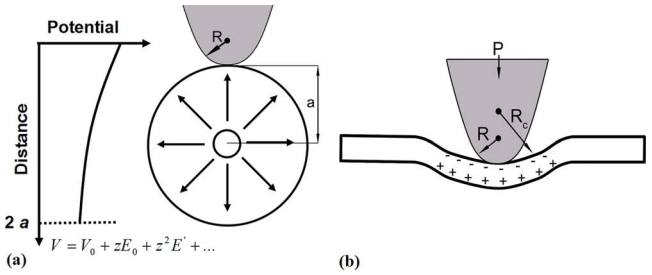

FIG. 3. (a) Intrinsic electromechanical response due to the piezoelectric effect in viral structure. Due to the intrinsic symmetry of the structure, the contributions due to the electric field are canceled and only the contribution due to the gradient term is nonzero. (b) Signal generation due to the flexoelectric effect. In this case, signal is generated only at the indented interface, resulting in more effective mechanism for electromechanical coupling.

The observation of electromechanical activity in TMV particles is somewhat unexpected since the structure has a helical symmetry. Here, we analyze two possible intrinsic mechanisms for electromechanical response of the cylindrical structure. The first is based on the nonuniform field below the AFM tip, which results in a nonzero piezoelectric response due to the incomplete compensation by opposing walls. This can be both due to the intrinsic piezoelectric properties of proteins forming the virus shell and surface piezoelectricity due to the presence of carboxyl groups on the outside and amino groups in the inside of the shell. The second is the flexoelectric coupling in a virus shell, as illustrated in Fig. 3. In this case, mechanical deformation of the shell gives rise to a dipole moment proportional to local curvature, and hence electromechanical response. For this analysis TMVs are considered as elastic rods similar to the model in Ref. 14.

Using the one-dimensioanl (1D) model developed by Ganpule *et al.*,[15] the piezoelectric response is approximated as

$$PR = \int_{-a}^{a} d_{33}(z) E_3(z) dz, \tag{1}$$

where, for a radially polarized piezoelectric cylinder, $d_{33}(z) = d_{\text{eff}}$ with $a > z > 0$, and $d_{33}(z) = -d_{\text{eff}}$ for $0 > z > -a$. Expanding the electric field below the tip as $E_3(z) = E_3^0 + zE_3'$, where $E_3' = \partial E_3 / \partial z$, valid for $R > a$, where R is the radius of the curvature of the tip, the piezoresponse can be estimated as $PR = d_{\text{eff}} a^2 E_3'$. Finally, using the spherical model for the tip, the electric field gradient can be estimated as $E_3' = V_{\text{tip}}/R^2$, giving rise to the effective piezoresponse signal, $PR_p = d_{\text{eff}} a^2 / R^2$.

A second possible mechanism for the linear electromechanical coupling in nanosystems is the flexoelectric effect, i.e., the linear coupling between the strain gradient and polarization (direct flexoeffect), and electric field and curvature. The analysis of the flexoelectric coupling in biomembranes has been reported by Petrov and Sachs,[16] who related the voltage-dependent indentation ΔR to the membrane thickness h, as $\Delta R / R_c = R f_m V_{\text{tip}} / (hK)$, where $K = Eh^3 / [12(1 - \sigma^2)]$ is membrane stiffness, E is Young's modulus, and σ is Poisson's ratio. The elastic constants for TMVs can be found in Ref. 14. The membrane flexoelectric coefficient f_m is related to the bulk flexoelectric constant f, as $f_m = fh$. The tip induced radius of curvature is related to the indentation force as $R_c = 4\pi K / P$, where P is indentation force. From this

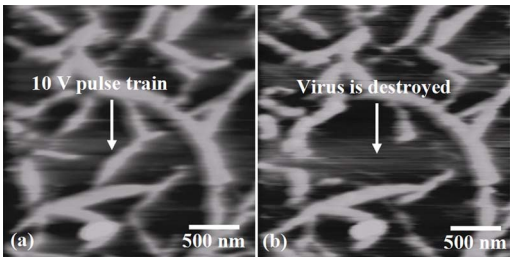

FIG. 4. Electrical manipulation of the virus. Surface topography (a) before and (b) after 10 V pulse train, demonstrating destruction of a defined virus particle.

analysis, the flexoelectric contribution to the piezoresponse signal is estimated as $PR_f = 16\alpha\pi^2 K f_m / P^2$, where $\alpha = V_v / V_{\text{tip}}$ and V_v is the potential drop across the virus.

Next, we estimate the relative contributions of the piezoelectric and flexoelectric responses to the PFM signal. For a spherical tip model with a tip radius of $R = 80$ nm as estimated from the topographic images, the potential drop across the virus shell is $V_v = aV_{\text{tip}}/R_c$ and thus $\alpha \approx 0.11$. The piezoelectric contribution to the signal can be estimated from $d_{\text{eff}} = 10$ pm/V (the same order of magnitude as for piezoelectric coupling in biopolymers) as $PR_p = 0.13$ pm/V. Young's modulus for TMV was found to be ~1 GPa, consistent with other measurements of similar macromolecular biological materials.[17] Estimating $\sigma = 0.33$, the membrane stiffness is $K = 6.82 \times 10^{-17}$ Nm. Using the order of magnitude estimate of $f = 1.1 \times 10^{-10}$ C/*m*, the flexoelectric contribution to the PFM signal is $PR_f = 12$ pm/V. Note that for biological systems the flexoelectric response can be significantly stronger than the piezoelectric one. For soft systems such as biomembranes, a response as large as several nm/mV has been observed.[18] However, even for relatively stiff virus particles, the flexoelectric response is expected to dominate electromechanical coupling.

PFM can be used not only for imaging but also for manipulation of the biological systems. Shown in Fig. 4 is the surface topography of a virus network before [Fig. 4(a)] and after [Fig. 4(b)] application of a 10 V_{pp} pulse train to a selected virus. Note that the application of a high bias resulted in the destruction of the selected virus [arrow in Fig. 4(b)].

To summarize, we have demonstrated electromechanical imaging of TMV viruses using the piezoresponse force microscopy. The PFM images show high resolution details invisible in the topographic images. The intrinsic electromechanical response has been analyzed using piezoelectric and flexoelectric models. It is suggested that, in this system, the flexoelectric response dominates the overall electromechanical response. We have also demonstrated electrical manipulation of this nanoscale biological system. The results obtained are important for the proposed applications of TMVs as biological templates for nanofabrication.

The research in ORNL has been supported by ORNL SEED SVK. The UCR researchers acknowledge the financial and program support of DARPA-SRC MARCO and its Focus Center on Functional Engineered Nano Architectonics (FENA).

[1] E. Fukada, Biorheology **32**, 593 (1995).
[2] C. Halperin, S. Mutchnik, A. Agronin, M. Molotskii, P. Urenski, M. Salai, and G. Rosenman, Nano Lett. **4**, 1253 (2004).
[3] S. V. Kalinin, B. J. Rodriguez, S. Jesse, T. Thundat, and A. Gruverman, Appl. Phys. Lett. **87**, 053901 (2005).
[4] A. K. Tagantsev, Phys. Rev. B **34**, 5883 (1986).
[5] W. E. Brownell, A. A. Spector, R. M. Raphael, and A. S. Popel, Annu. Rev. Biomed. Eng. **3**, 169 (2001).
[6] W. Shenton, T. Douglas, M. Young, G. Stubbs, and S. Mann, Adv. Mater. (Weinheim, Ger.) **11**, 253 (1999).
[7] C. E. Flynn, S. W. Lee, B. R. Peelle, and A. M. Belcher, Acta Mater. **51**, 5867 (2003).
[8] W. L. Liu, K. Alim, A. A. Balandin, D. M. Mathews, and J. A. Dodds, Appl. Phys. Lett. **86**, 253108 (2005).
[9] A. Gruverman, O. Auciello, and H. Tokumoto, Annu. Rev. Mater. Sci. **28**, 101 (1998).
[10] L. M. Eng, S. Grafstrom, Ch. Loppacher, F. Schlaphof, S. Trogisch, A. Roelofs, and R. Waser, Adv. Solid State Phys. **41**, 287 (2001).
[11] S. V. Kalinin, E. Karapetian, and M. Kachanov, Phys. Rev. B **70**, 184101 (2004).
[12] Yu. G. Kuznetsov, A. J. Malkin, T. A. Land, J. J. DeYoreo, A. P. Barba, J. Konnert, and A. McPherson, Biophys. J. **72**, 2357 (1997).
[13] C. Möller, M. Allen, V. Elings, A. Engel, and D. J. Müller, Biophys. J. **77**, 1150 (1999).
[14] V. A. Fonoberov and A. A. Balandin, Phys. Status Solidi B **241**, R67 (2004); J. Biomed. Nanotech. **1**, 90 (2005).
[15] C. S. Ganpule, V. Nagarjan, H. Li, A. S. Ogale, D. E. Steinhauer, S. Aggarwal, E. Williams, R. Ramesh, and P. De Wolf, Appl. Phys. Lett. **77**, 292 (2000).
[16] A. G. Petrov and F. Sachs, Phys. Rev. E **65**, 021905 (2002).
[17] M. R. Falvo, S. Washburn, R. Superfine, M. Finch, F. P. J. Brooks, V. Chi, and R. M. I. Taylor, Biophys. J. **72**, 1396 (1997).
[18] R. M. Raphael, A. S. Popel, and W. E. Brownell, Biophys. J. **78**, 2844 (2000).